REVIEW

Check for updates

Surface plasmon resonance of Au/Ag metals for the photoluminescence enhancement of lanthanide ion Ln^{3+} doped upconversion nanoparticles in bioimaging

Hao Peng,[ab] Shunxiang Li,[a] Jie Xing,[ac] Fang Yang [ID] *[ac] and Aiguo Wu [ID] *[ac]

Deep tissue penetration, chemical inertness and biocompatibility give UCNPs a competitive edge over traditional fluorescent materials like organic dyes or quantum dots. However, the low quantum efficiency of UNCPs becomes an obstacle. Among extensive methods and strategies currently used to prominently solve this concerned issue, surface plasmon resonance (SPR) of noble metals is of great use due to the agreement between the SPR peak of metals and absorption band of UCNPs. A key challenge of this match is that the structures and sizes of noble metals have significant influences on the peak of SPR formants, where achieving an explicit elucidation of relationships between the physical properties of noble metals and their SPR formants is of great importance. This review aims to clarify the mechanism of the SPR effect of noble metals on the optical performance of UCNPs. Furthermore, novel research studies in which Au, Ag or Au/Ag composites in various structures and sizes are combined with UCNPs through different synthetic methods are summarized. We provide an overview of improved photoluminescence for bioimaging exhibited by different composite nanoparticles with respect to UCNPs acting as both cores and shells, taking Au@UCNPs, Ag@UCNPs and Au/Ag@UCNPs into account. Finally, there are remaining shortcomings and latent opportunities which deserve further research. This review will provide directions for the bioimaging applications of UCNPs through the introduction of the SPR effect of noble metals.

10th Anniversary Statement

Over the past ten years, *Journal of Materials Chemistry B* has achieved considerable developments. More than 200 articles related to upconversion nanoparticles (UCNPs) have been published since 2013 when the research was focused on cancer cell imaging and death, and has recently shifted to multimodal theranostics of tumors *in vivo*. Wu's group has also made some progress in the fluorescence imaging of Ln^{3+}-doped nanoparticles but encountered the problem of insufficient quantum efficiency. In this review, a combination of the surface plasmon resonance effect of novel metals Au/Ag and Ln^{3+}-doped UCNPs has been proved to be practicable in fluorescence enhancement which can be explained using three plausible mechanisms. Au/Ag–UCNP composites fabricated by physical approaches exhibit superior enhancement factors but less flexibility and biocompatibility, while Au/Ag–UCNP systems synthesized chemically improve the disadvantages but with hard-to-control fluorescence enhancement. This manuscript therefore emphasizes the urgent need to develop an efficient and biosafe preparation method. In addition, this review covers the applications of Au/Ag–UCNPs in bioimaging from upconversion luminescence imaging agents to multi-modal imaging agents in tumor-bearing mice. Hence, the strategy of noble metal enhanced UCNPs has been proven to be feasible and has prospects for bioimaging applications like accurate tumor diagnosis and surgery guidance.

[a] *Cixi Institute of Biomedical Engineering, International Cooperation Base of Biomedical Materials Technology and Application, Chinese Academy of Science (CAS) Key Laboratory of Magnetic Materials and Devices and Zhejiang Engineering Research Center for Biomedical Materials, Ningbo Institute of Materials Technology and Engineering, CAS, Ningbo, 315201, P. R. China. E-mail: yangf@nimte.ac.cn, aiguo@nimte.ac.cn*

[b] *University of Chinese Academy of Sciences, No. 1 Yanqihu East Road, Huairou District, Beijing, 101408, China*

[c] *Advanced Energy Science and Technology Guangdong Laboratory, Huizhou, 516000, China*

Introduction

The concept of upconversion luminescence was first discovered by Bloembergen in 1959.[1] Afterwards, Auzel pointed out in his study that when Tm^{3+},Er^{3+} and Ho^{3+} were co-doped with Yb^{3+} in ytterbium sodium tungstate glass, the excitation light intensity under infrared light increased by nearly two orders of magnitude, formally proposing the concept of upconversion luminescence.[2] However, it was not until the past two decades

that the application of upconversion luminescence materials developed rapidly, along with the exponential growth of the publication of relevant papers.[3] Upconversion nanoparticles (UCNPs) are a class of materials with anti-Stokes luminescence properties, and exhibit continuous absorption of two or more low-energy pumped photons by excited state absorption (ESA), energy transfer upconversion (ETU), photon avalanche (PA), cooperative energy transfer (CTE) and energy migration-mediated upconversion (EMU), thus releasing photons with higher energy.[3,4]

Compared with conventional organic fluorescent dyes and quantum dots, UCNPs have better chemical stability, reducing the occurrence of photobleaching.[5] Meanwhile, multi-wavelength emission can be achieved by adjusting both the matrix and doping ions due to their independence from the crystal size and structure.[6–8] On the other hand, UCNPs excited by near-infrared irradiation can effectively solve the problems of poor tissue penetration, biological toxicity and self-fluorescence interference of organic fluorescent dyes and quantum dots.[5,9] Considering the above advantages as well as long fluorescence life, UCNPs have been widely applied in biological imaging,[9–13] therapy[14–17] and biomarkers as ideal functional materials.[18–21]

One of the most important indexes to evaluate the optical properties of upconversion materials is fluorescence quantum efficiency (QE), which can be calculated by the ratio of emitted to absorbed photons.[22] Unfortunately, the limited absorption cross section and large specific surface area of UCNPs, as well as surface defects, result in low luminescence efficiency,[23] usually no more than 1% as reported,[24] restricting the further application of UCNPs severely. Moreover, there is an intensity threshold (from the ground state to excited states) for the

Hao Peng

Hao Peng (male) is a PhD student at the Cixi Institute of Biomedical Engineering, Ningbo Institute of Materials Technology and Engineering, Chinese Academy of Sciences (CIBE-NIMTE). He obtained his Bachelor's degree in Materials Science and Engineering from the University of the Chinese Academy of Sciences in 2018 and his Master's degree in Materials Science and Engineering from the National University of Singapore in 2020. At present, he is studying at the CIBE-NIMTE for his PhD degree in the areas of lanthanide ion doped optical upconversion nanoparticles and their bioimaging application.

Shunxiang Li

Shunxiang Li is currently working as a research assistant at the Cixi Institute of Biomedical Engineering, Ningbo Institute of Materials Technology and Engineering, Chinese Academy of Sciences, and doing majors in mechanical engineering.

Jie Xing

Jie Xing obtained her PhD from the Ningbo Institute of Materials Technology and Engineering, Chinese Academy of Sciences and is now carrying out her post-doctoral work at NIMTE. Her research interests are focused on the development of fluorescent probes for tumor diagnosis and therapy.

Fang Yang

Fang Yang is the master supervisor as well as an associate professor at the Ningbo Institute of Materials Technology and Engineering, Chinese Academy of Sciences. He received bachelor's and master's degrees in Physics and PhD in Physical Chemistry from the University of Marburg, Germany. He is currently a member of the European Cooperation in Science & Technology Organizing Committee as well as the Youth Innovation Promotion Association of CAS. He is committed to the development of functional nanomaterials, their physical and chemical properties and biological applications, based on which he has published over 40 original articles with a high peer reputation.

This journal is © The Royal Society of Chemistry 2023

J. Mater. Chem. B, 2023, **11**, 5238–5250 | **5239**

occurrence of nonlinear luminescence upconversion.[25] Meanwhile, according to the data from "American National Standard for Safe Use of Lasers", radiation light in the near-infrared band with power above 0.726 W cm^{-2} is harmful to biological tissue,[26] which sets the maximum value of excitation light utilized in biological applications. Therefore, the development of UCNPs with both low excitation threshold and high luminescence intensity has become a hotspot and difficulty in biomedical research.[27]

Through years of exploration, researchers have discovered ways to effectively modify UCNPs, briefly divided into two types. One approach is internal regulation, including matrix lattice[28–30] and doping ions.[9,31] The other is to regulate the external environment of UCNPs, such as surface passivation[32,33] commonly and metal surface plasmon resonance (SPR).[34–36] Zhan[37] utilized gold nanorods (GNRs) to enhance, by up to 35 000 times, the upconversion emission, demonstrating the great potential of the metal-SPR method.

Mechanism of SPR enhanced upconversion

Mechanism of upconversion luminescence

UCNPs are generally composed of a host matrix, a sensitizer and an activator. The most widely used host matrix is NaYF$_4$ in the hexagonal phase[38] because of its ample interspace for doping ions, favourable light transmission and low phonon energy, which reduce the energy loss of the exciting radiation. Trivalent lanthanide ions are ideal elements for both a sensitizer (such as Neodymium, Nd^{3+} for 808 nm;[39] Ytterbium, Yb^{3+} for 980 nm[38]) and an activator (such as Holmium, Ho^{3+},[40] Thulium, Tm^{3+},[41] and Erbium, Er^{3+},[42]). The occurrence of upconversion luminescence requires that the doping ions inside UCNPs have abundant long-life intermediate energy levels (Fig. 1(a)) to promote the ETU process between sensitizers and activators.

Aiguo Wu received his PhD degree in 2003 from Changchun Institute of Applied Chemistry, CAS, supervised by Prof. Erkang Wang and Prof. Zhuang Li. He started his independent career working for NIMTE after taking up his research associate appointment at Northwestern University (Prof. Gayle E. Woloschak's group), USA, and his postdoctoral positions at Caltech (Prof. Ahmed Zewail's group), USA, and the University of Marburg (Prof. Norbert A. Hampp's group),

Aiguo Wu

Germany. His research focused on biomedical nanoprobes and their application. He has authorized over 290 scientific publications which have been cited more than 14 700 times with an H-index of 61.
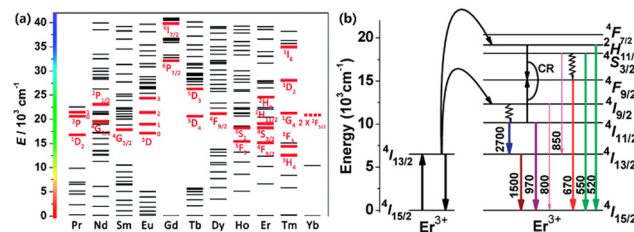
Fig. 1 (a) Partial energy level diagrams of Ln^{3+}. Corresponding typical UC emissive excited levels are highlighted with red bold lines; reproduced from ref. 4 with permission from the Royal Society of Chemistry. (b) Diagram of the energy levels of the Er^{3+} ion and the proposed mechanisms of upconversion. Adapted with permission from ref. 43. Copyright {2022} American Chemical Society.

The outermost electron configuration of Er, one of the lanthanide elements, is 4f^{12}5s^{2}5p^{6}6s^2. Under the combination of Coulomb interaction, spin–orbital coupling and crystal field disturbance, the 4f^n electron configuration is divided into several intermediate energy levels.[38] When Er single-doped UCNPs are exposed to 1550 nm NIR-II photons, Er^{3+} ions can be excited from the ground state ^{4}I$_{15/2}$ to ^{4}I$_{13/2}$ through the ESA process,[4] whereafter, another absorbed photon can excite the ions into ^{4}I$_{9/2}$, some of which are dropped to the ground state, resulting in the emission of 800 nm photons. The further ESA process stimulates ^{4}I$_{9/2}$ ions to higher ^{2}H$_{11/2}$. As a consequence, the excited ions emit green photons through a radiative transition to the ground state or transit to the ^{4}F$_{9/2}$ state and perform red emission (Fig. 1(b)).[43] As for Yb^{3+}/Er^{3+} co-doped UCNPs, Yb^{3+} ions are firstly excited to ^{2}F$_{5/2}$ by the ESA process with absorption at 980 nm. Since the energy barrier in Yb^{3+} ions from ^{2}F$_{5/2}$ down to the ground state ^{2}F$_{7/2}$ matches the energy difference between intermediate energy levels (^{4}I$_{15/2}$ 5/^{4}I$_{11/2}$, ^{4}I$_{15/2}$ → ^{4}I$_{11/2}$) in Er^{3+} ions, an effective ET process helps to excite nearby Er^{3+} ions into ^{4}I$_{11/2}$ or one of the higher energy levels ^{4}F$_{7/2}$ through a continuous process.[44] Hence, for co-doping UCNPs, sensitizers can absorb quantities of photons, increasing the ESA process which is weak and even negligible in single doped UCNPs[45] while the ET between sensitizer ions and activator ions causes energy loss as well. Corresponding to the statement above, it is significant to develop practical routes to improve the luminescence efficiency of UCNPs.

Mechanism of the plasmon resonance effect

The plasmon resonance effect of noble metals with nano sizes (usually Silver, Ag and Gold, Au), also known as localized surface plasmon resonance (LSPR), refers to the continuous oscillation of electrons in the conduction band of noble metals under the circumstance of illumination with electromagnetic radiation, resulting in a dense wave of electrons propagating along the metal surface.[46] In the case of light radiation or an applied electric field, the surface electrons collectively vibrate and emit an electromagnetic wave. When the free electron field produced by the electron vibration couples with the wavelength of incident light, the LSPR effect whereby the energy of the incident light is focused or transferred on the metal surface

5240 | J. Mater. Chem. B, 2023, 11, 5238–5250

This journal is © The Royal Society of Chemistry 2023

takes place,[47] and scattering or absorption enhancement occurs at the particle. It can be noticed that LSPR will occur only if the incident light wavelength exceeds the particle size. As an example, bulk Au material has a golden color, whereas Au NPs appear deeply ruby-red.[48] Here, the absorption of photons exceeds light reflection.[49]

The absorption and scattering characteristics of noble metal particles in the visible band have been discovered and utilized by intelligent humans since ancient Rome, where wine glass doped with noble metal particles revealed gorgeous colors in the sunlight.[50] But it was not until 1908 that Gustav Mie explained the chromatic dispersion properties of noble metal ions through Maxwell's equations.[51] The Mie theory is an analytical solution to Maxwell's equations for electric field scattering operation, mainly used for spherical noble metal particles with wavelength-similar sizes.[52] In addition to calculating the scattering of a single spherical noble metal particle, Mie theory can also be applied to calculate multiple metal particles. Since Pines proposed the term 'Plasmon' to describe this phenomenon,[53] mathematical methods such as finite difference time domain (FDTD), discrete dipole approximation (DDA) and finite element method (FEM) have been commonly used to study its nature. In 1957, Swan and Powell experimentally confirmed the surface electron oscillation mode of noble metals calculated by Ritchie,[54] after which the name 'surface plasmon' formally appeared.[55]

According to theoretical calculation models like the Drude model,[56,57] the oscillation frequency of metal particles is related to the dielectric constant and the damping coefficient of metals. In addition, Mie's equation also indicates the connection between the position of the LSPR spectrum and the size and morphology of metal particles. The position of the resonance peak appears to red shift with the increase of particle size as reported.[58,59]

Mechanism of plasmon enhancement of UCNPs

Enhancing upconversion materials by using plasmon resonance is recognized as one of the most effective methods to improve luminescence intensity. Yan Chunhua et al. first reported the application of SPR enhancement in upconversion luminescence of rare earth fluorides[60] where they fabricated Ag nanowire-NaYF$_4$: Yb^{3+},Er^{3+} composites by a self-assembly approach. The absorption peak of Ag nanowires lay around 420 nm which was different from the spectrum of pure NaYF$_4$: Yb^{3+},Er^{3+} particles. The results showed that the emission intensity of composites at 543 nm (green emission) and 659 nm (red emission) under 980 nm excitation increased by 3.7 and 2.3 times, respectively.

Actually, SPR-enhanced upconversion luminescence refers to the phenomenon that when UCNPs are in proximity to the surface of noble metals, the metal LSPR interacts with the UCNPs, resulting in a significant increase in the photoluminescence intensity of the UCNPs compared to that of the free state.[61] In general, the enhancement can be achieved only if the metal is kept at an appropriate distance from the UCNPs. Shen et al.[62] found that the best thickness of a SiO$_2$ layer
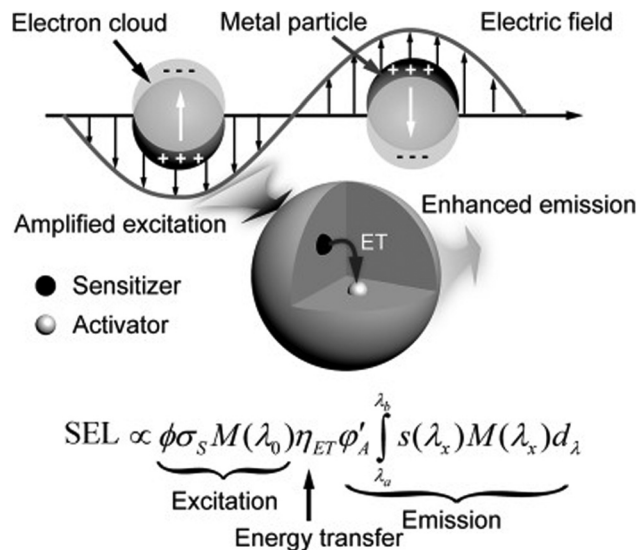

Fig. 2 Schematic illustration showing the plausible mechanism that governs the plasmonic enhancement of upconversion luminescence.[65]

sandwiched between Ag nanoparticles and NaYF$_4$: Yb,Er,Gd was 15 nm with an enhancement factor of 3.4. When Ag particles and NaYF$_4$ UCNPs approached a distance below 5 nm, the activator ions in UCNPs easily diffuse to the surface,[63] leading to electron countercurrent with metal ions at the Fermi level,[64] causing a severe surface quenching effect. As for a far distance, the Ag SPR effect did not interact with both the absorption and emission of NaYF$_4$ UCNPs.

So far, SPR enhanced upconversion can be basically explained by the following three mechanisms:[65–69] excitation enhancement, emission enhancement and energy transfer, as shown in Fig. 2.

The SPR effect of metal nanostructures enhances the local electric field, which is coupled with UCNPs, thus amplifying the absorption of the sensitizer.[70] Better performance can be realized if the excitation wavelength matches the strongest extinction of the SPR effects. The luminescence intensity I of UCNPs is estimated using the following equation

$$I \propto |E|^2 \times \sigma_s \times \eta_{ET} \times \psi_A$$

where E is the electric field intensity, σ_s is the absorption cross-section, η_{ET} is the energy transfer efficiency from sensitizers to activators, and ψ_A is the quantum yield of the activator.

Therefore, when UCNPs are anchored near metal nanoparticles, the SPR effect of the metal generates a strong local electric field, and the boosted electric field intensity E expands the flux of incident light ϕ, thus increasing the light absorption by UCNPs, and finally improving the luminescence intensity.

Emission enhancement will take place when the oscillation frequency of metal SPR overlaps with the luminous band of UCNPs. The coupling of the emitted light and the SPR effect can magnify the local state density of photons near the metal surface.[65] Subsequently, the radiation decay rate of the activator is improved so as to increase luminous intensity.[71,72]

The addition of metal nanoparticles fastens the radiative transition rate of the UCNP activator, advancing the quantum yield while reducing the fluorescence lifetime, and eventually enhancing upconversion emission.

Besides, Nagpal et al.[73] coupled $NaYF_4$:Yb^{3+},Er^{3+} nanoparticles with Au pyramid nanostructures, which implies that the SPR effect can accelerate the energy transfer between sensitizer and activator pairs in UNCPs. For a certain SPR–UCNP system, the upconversion enhancement is conventionally controlled by one of three mechanisms. For instance, Zhang[74] synthesized Au–$NaYF_4$ core–shell nanostructures where the emission enhancement mechanism by the Au nanoshell contributed to upconversion improvement. Besides, there may be two or even three mechanisms working together to promote the enhancement. Both Kang[75] and He[76] reported that Au nanorod plasma can enhance excitation and emission simultaneously in Au nanorod@SiO_2@UCNP composites (Fig. 3). By adjusting the aspect ratio of Au nanorods, the longitudinal SPR wavelength can be efficiently shifted from visible to near-infrared light fitting the excitation wavelength of sensitizers. The transverse SPR remains at 530 nm, matching the green emission band of the activator Er^{3+}, thus selectively accelerating the radiative decay in green upconversion. However, the three mechanisms stated above are still related to the interaction between the SPR effect and electromagnetic waves substantially. At present, there is no recognized explanation for the deep mechanism of the metal SPR effect enhancing UCNP luminescence.
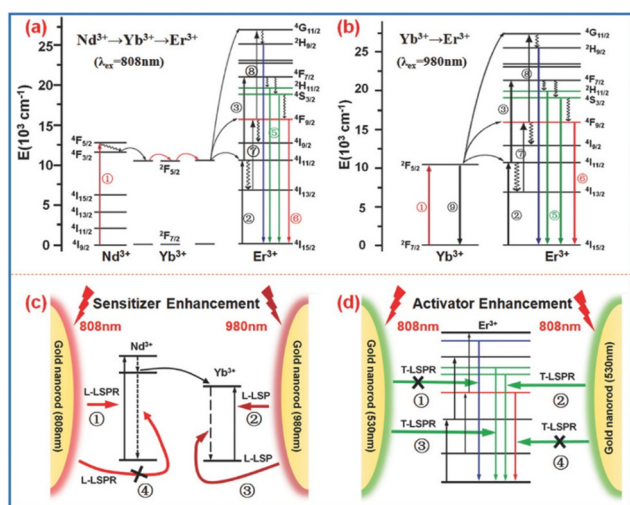

Fig. 3 (a and b) The energy diagrams of Nd^{3+}, Yb^{3+}, and Er^{3+} ions undergoing ETU upon excitation at 808 and 980 nm, respectively. (c) The GNR Longitudinal-LSPR-induced absorption enhancement for an Nd^{3+} ion upon excitation at 808 nm and for a Yb^{3+} ion upon excitation at 980 nm. The radiative decay rate of the Yb^{3+} ion is also accelerated by the GNR Longitudinal-LSPR (due to energy matching) while that of the Nd^{3+} ion is not (denoted by " ×") because of the fast phonon-mediated relaxation and energy migration to the Yb^{3+} ion. (d) The GNR Transverse-LSPR-induced green-emission enhancement for both ions upon excitation at 808 nm. The blue and red emissions are not affected by the GNR Transverse-LSPR due to energy mismatch (denoted by " ×").[75]

Construction methods of the metal-UCNP system

As described above, the SPR–UCNP interaction is closely related to the distance. In order to accurately control the distance between UCNPs and metal, most of the literature adjusts the concentration and size of the metal[77–80] or introduces an intermediate layer[74,81–84] to achieve the best enhancement performance. So far, SPR–UCNP systems are mostly built either by chemical methods or physical approaches.

Physical construction of SPR–UCNPs

Self-assembly method

The most basic physical construction method is to deposit metal and UCNPs directly on the surface of the substrate (generally glass). Metal-UCNP nanocomposites can be self-assembled after the solvent evaporates.[85] Zhang and co-workers[86] took an optical microfiber prepared by flame heating as a template, sprayed the Au nanofilm onto its surface by rotation and then dropped the aqueous solution of UCNPs. UCNPs/Au samples were fabricated after evaporation. The UCNPs/Au composites displayed enhanced emission at 523 nm under 980 nm excitation, 35 times stronger than that of the original UCNPs. The mechanism could be attributed to the excitation enhancement from the SPR effect instead of emission enhancement because there was only a slight change in the lifetimes of emissions after the Au modification, standing for the invariant radiative decay rate (Fig. 4b–d).

Subtly, Xue[78] and Shao[87] spin-coated the solution of Au nanorods and UCNPs on the same glass substrate and evaporated it in a vacuum. Then, Xue used atomic force microscopy (AFM) to identify the locations of gold nanorods and UCNPs, and propelled UCNPs with AFM probes until the gold nanorods joined. The whole process was monitored under a confocal laser microscope, which assisted in optical emission spectrum measurement, revealing that the red upconversion intensity was increased by 110 fold and 19 fold joined with Au nanorods with a large diameter (46.7 nm) or a small diameter (27.3 nm). The experimental data and finite-difference-time-domain
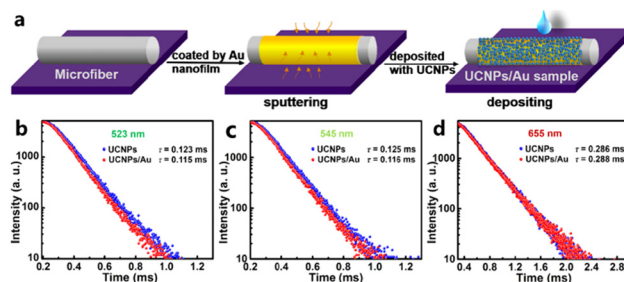

Fig. 4 (a) Formation process of the UCNPs/Au sample. (b–d) Decay curves of $^2H_{11/2}$–$^4I_{15/2}$ (523 nm), $^4S_{3/2}$–$^4I_{15/2}$ (540 nm) and $^4F_{9/2}$–$^4I_{15/2}$ (655 nm) transition of Er^{3+} ions in UCNPs/Au and UCNPs samples, respectively. Adapted with permission from ref. 86. Copyright {2022} American Chemical Society.

5242 | J. Mater. Chem. B, 2023, **11**, 5238–5250

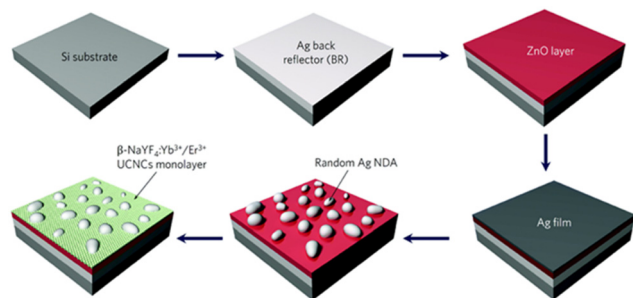This journal is © The Royal Society of Chemistry 2023

Fig. 5 A schematic illustration of the fabrication procedure of the plasmonic back-reflector substrate on which a dewetted Ag nanodome array (NDA) and a monolayer of upconversion nanocrystals are mounted. Reproduced from ref. 89 with permission from the Royal Society of Chemistry.

calculation ensure the combination of excitation and emission enhancement mechanisms. The Shao group first synthesized porous Ag nanofilms based on polystyrene microspheres and dispersed $NaYF_4$: Yb^{3+},Er^{3+} nanoparticles, fabricated in the traditional way,[88] using a spin coater. After the solvent evaporated, a 60-fold increase in green emission (540 nm) and a nearly 50-fold increase in red emission (668 nm) were detected. Lee[89] designed a plasmonic Ag nanodome array (NDA)-UCNP structure by spin coating as well, which could attain as high SPR enhancement as 800 and 340 times at 656 nm and 542 nm under weak excitation power, separately, as shown in Fig. 5.

Liu et al.[90] fabricated a hybrid composed of Al disk/SiO_2/UCNPs/Al film through a series of physical processes like electron beam deposition, spin coating and developing processing. The maximum enhancement factors of the final products in green (545 nm) and red bands (655 nm) were 90 and 180, respectively. In addition, they have noticed that the SPR effect of Al disks has significantly different influences on green and red emissions (Fig. 6). The hybrids exhibit the strongest red signals at 170 nm diameter of Al disks. However, when the diameter of the Al disks is enlarged to 210 nm, green emission dominates the luminescence with the highest enhancement factor.

Periodic metal nanostructures

The direct deposition or spin-coating method is convenient but the nanoparticles tend to agglutinate during the solvent volatilization process, which makes it difficult to ensure uniformity on the substrate. Therefore, periodic metal nanostructures such as nanogratings, nanoholes, nanorods and triangular arrays prepared by template etching and nano-imprint technology have
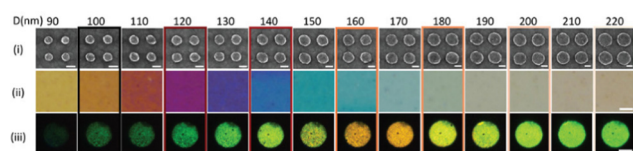
been introduced into the SPR–UCNP nanocomposites. Good periodicity, controllable geometry and nanoscale precision can better exert the metal SPR effect due to a transverse momentum.[91] As reported, both periodic gold nanorods or gold nanoholes enhanced upconversion intensity over 35 fold.[92,93]

A nanohole array is one familiar periodic nanostructure. As shown in Fig. 7a, Zhan coupled plasmonic Au-nanohole–nanoplate bilayer arrays (PABAs) with core–shell nanoparticles.[94] The results demonstrated a 6-fold increase in the green emission of core–shell UCNPs after coupling, which was proportional to the irradiation intensity from 12.5 to 50 mW mm^{-2}, arising from a stimulated local electric field of PABAs and coherent interference of the SPR effect with the emission band. Similarly, but further, Das and his group synthesized dispersible metal–insulator–metal (MIM) structures (inset in Fig. 7b),[95] where Au nanohole arrays were constructed utilizing the template method. UCNPs were encapsulated in an insulator layer and coupled with top and bottom Au layers. From the upconversion spectra in Fig. 7b, the photoluminescence intensity was demonstrated to be strongly heightened at the 250 nm diameter of MIM composites. Moreover, it is noteworthy that a relatively low excitation power density (<50 W cm^{-2}) induced green emission with over 1000 times enhancement while the factor was no more than 200 at a power density exceeding 20 kW cm^{-2} (Fig. 7c), which shows potential in sensitive and effective theranostics of lesions with mild side effects.

Chu[96] obtained a periodic Ag nanograting through photochemical reduction on a polyimide layer and a Ag nanofilm as a control. The period of the Ag nanograting is precisely managed by the regulation of the angle at which the Ag stock solution is exposed to the laser and reduced. The strongest enhancement of the SPR effect on UCNP luminescence is at the nanograting period of 700 nm, with a factor of 4.5 totally, two times higher than that of non-periodic Ag nanofilms. It can be attributed to a broad absorption of Ag nanograting-UCNPs at the NIR region, resulting from the Ag SPR effect.
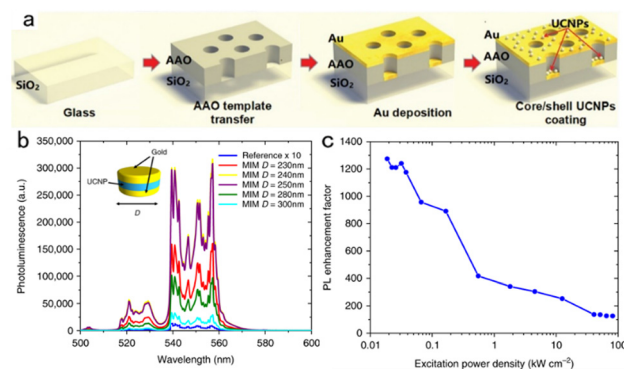

Fig. 6 SEM (i), reflected bright field (ii), and upconversion luminescence (iii) color patches of pixel arrays with D = 90–220 nm and s = 100 nm.[90]

Fig. 7 (a) The fabrication process of the AAO@Au@CS-UCNPs.[94] (b) Green emission spectra of the reference sample and the (MIM) structure of varying diameters under 980 nm excitation. The reference sample emission is magnified by 10 to show the relevant features. Inset: Schematic of the MIM nanostructure. (c) 250 nm diameter MIM PL enhancement as a function of power density.[95]
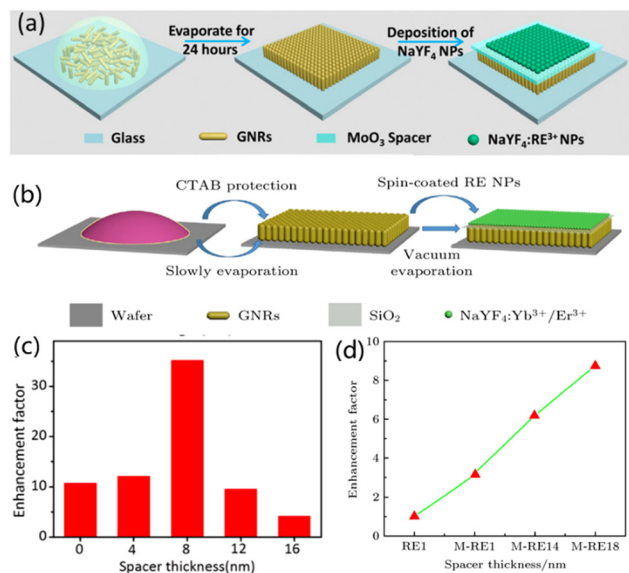
Fig. 8 (a and b) Schematic illustration of the fabrication process of NaYF$_4$:Yb^{3+},Er^{3+}/MoO$_3$/GNRs and GNRs@SiO$_2$@NaYF4:Yb^{3+}/Er^{3+}, respectively. (c and d) The enhancement factors as a function of the MoO$_3$ or SiO$_2$ spacer thickness. Adapted with permission from ref. 92. Copyright {2022} American Chemical Society and ref. 97.

Lanthanide ion doped UCNPs uniformly coated on the neatly arranged vertical Au nanorod (GNR) substrate under rotation also show upconversion emission improvement with 8.8-fold and 35-fold maxima, adjusted by the thickness of the intermediate layer (SiO$_2$ and MoO$_3$ shown in Fig. 8) between the GNR and UCNPs under 980 nm excitation,[92,97] respectively. GNR absorption peaks are located at 520 nm and 680 nm, which are approximately coupled to Er^{3+} emission wavelengths of 540 nm and 640 nm. Besides, due to the vertical alignment characteristics of GNRs, the coupling effect between the SPR effect and the emission wavelength of red light ($^4F_{9/2}$–$^4I_{15/2}$) is larger than that of green light.[75]

Except for the standard circular arrays, other periodic metal nano-arrays in various shapes perform well in SPR enhancement too. Square aperture arrays of Au metal are reported to have an enhancement factor of 450 on the upconversion emission of Er^{3+} doped UCNPs, even better than the performance of Au annular aperture arrays, which is 370.[98] A fascinating Au pyramid array coupled with NaYF$_4$: Yb^{3+}/Er^{3+} nanoparticles was synthesized by Sun,[73] displaying a minimum factor of 6 of the SPR effect enhancement. Chen[36] prepared islands Au–Ag alloy films *via* the PMMA removal method with UCNPs self-assembled onto the surface and explored an optimal upconversion enhancement of the composites which is 180-fold.

However, though periodic metal structures have an outstanding upconversion enhancement effect on UCNPs, their processing equipment is expensive and not suitable for mass production. More critically, physical methods are mostly carried out on rigid substrates such as glass and silicon wafers, which lack flexibility and biocompatibility. Hence, the applications in biomedical fields are greatly limited.

Chemical synthesis of SPR–UCNPs

The simplest chemical synthesis method is to directly dope metal ions into UNCPs, currently used in rare earth ions doped phosphors.[99] With advanced research work, it is found that the morphology, size and concentration of metal particles as well as the distance between metal and UCNPs will affect the emission intensity, as mentioned above. Therefore, SPR–UCNP systems with core–shell structures synthesized in chemical approaches are mostly considered[100] which can make better use of the SPR effect of metal while reducing the energy loss from surface defects of UCNPs.[101]

Core–shell is an ordered structure formed by covering nanomaterials through chemical bonds, Coulomb electrostatic attraction, adsorption layer media and other interaction forces. Based on the different materials of the core and shells, SPR–UCNP systems can be separated into two types (Fig. 9): one is the core composed of UCNPs and the shell layer is composed of metal, while the inverted structures also hold. The former one is the current mainstream of plasmon-enhanced upconversion materials, since the surface defects are weakened and the SPR effect is greatly brought into play.

Duan's group studied the SPR effect of gold particle coverage on NaYF$_4$: Yb^{3+}, Tm^{3+} core[102] and the results revealed that with the increase of attached Au particles, the upconversion luminescence intensity gradually increases to the maximum value (1.5 times more than pure UCNPs). However, after the formation of an Au shell in Fig. 10, intensity started to decline with a thicker Au shell. Considering the distance between metals and UCNPs affects the enhancement,[62] an intermediate isolation layer is widely introduced in the compounds.

Ding and co-workers[103] took NaYF$_4$: Yb^{3+},Er^{3+} nanoparticles as the core and SiO$_2$-encapsulated Ag nanoparticles as the shell, fabricating the hybrid material with almost 3.5 times luminescence enhancement in both green and red emission. Yuan[104] set Ag nanoparticles free from the SiO$_2$ shell and designed a NaYF$_4$: Yb^{3+},Er^{3+}@SiO$_2$@Ag nanostructure. The addition of an Ag shell improved the photoluminescence intensity of NaYF$_4$: Yb^{3+},Er^{3+}, which depended on the thickness of SiO$_2$. The most significant enhancement appeared when the SiO$_2$ layer is regulated to 10 nm. Soon after, Shen[62] and Qin[81] proved the SPR enhancement of the Ag shell and the negative influence of
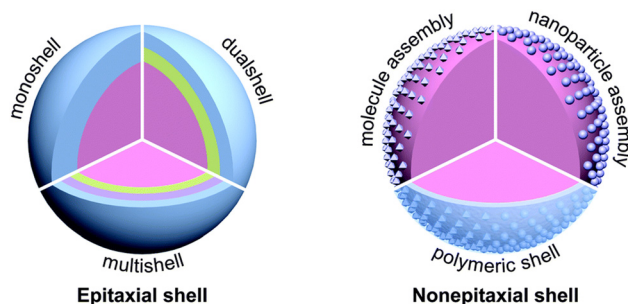

Fig. 9 Schematic illustration of the typical architectures of UC core–shell nanoparticles. Reproduced from ref. 100 with permission from the Royal Society of Chemistry.
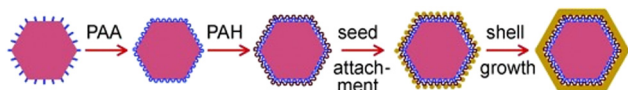
5244 | *J. Mater. Chem. B*, 2023, **11**, 5238–5250

This journal is © The Royal Society of Chemistry 2023

Fig. 10 Illustration of surface functionalization, gold NP attachment, and gold nanoshell growth on the upconversion nanoparticles.[102]

isolation layer thickness on the UCNPs core (Fig. 11), which can be attributed to the competition between energy transfer and radiation attenuation rate.

More interestingly, studies have revealed that the thickness of the metal shell which is usually made up of Ag and Au along with the thickness of the intermediate layer composed of SiO_2 affects the upconversion enhancement.[105] When the Au shell is 8 nm thick, its SPR peak located at 540 nm corresponds to the emission wavelength of UCNPs thus contributing to the enhancement factor of 9.1.[74] However, the SPR peak shifts to 900 nm with a 3 nm thick Au shell, enhancing full-wave luminescence by a factor of 2–3.[106]

Currently, for the sake of a higher enhancement factor of metal-UCNPs core–shell structures, Kang[75] regarded a sensitizer-doped host matrix $NaGdF_4$: Yb^{3+}, Nd^{3+} as another intermediate layer coating the luminous core $NaGdF_4$: Yb^{3+},Er^{3+}. Inside the core–shell UCNPs, the energy transfer can occur between Nd^{3+}–Yb^{3+}–Er^{3+} or Yb^{3+}–Er^{3+} ion pairs. Besides, on the surface of UCNPs, Au nanorods alongside SiO_2 layers are attached due to electrostatic interaction. Kang named the final Au–UCNPs composites core–shell–shell upconversion nanocrystals (UCNC). The Au Longitudinal-SPR wavelength couples with the irradiation wavelength at 808 nm if the thickness of the SiO_2 layer is 28 nm, increasing the local electrical field which is proportional to the square root of light flux. Thus because of the excitation enhancement mechanism, the signal intensity in green emission is 18.85 times greater than that of UCNPs without Au@SiO_2 shells.
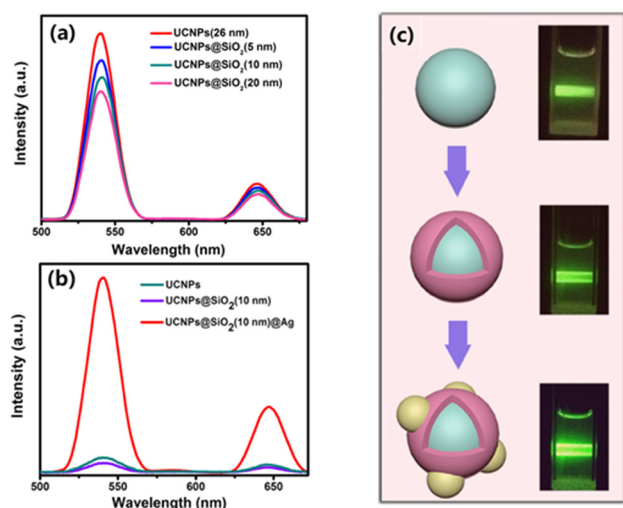

Fig. 11 (a) UC emission spectra of pure UCNPs and UCNPs@SiO$_2$ core/shell NPs. (b) UC emission spectra of the UCNPs, UCNPs@SiO$_2$(10 nm) NPs and UCNPs@SiO$_2$(10 nm)@Ag NPs. (c) Schematic illustrations of these three types of NPs and their digital luminescence photos.[81]
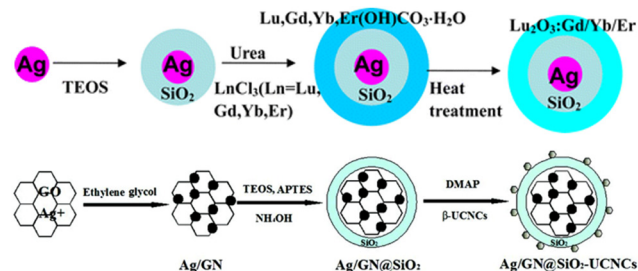

Fig. 12 Examples of the fabrication process of the metal core-UCNP shell nanostructures. Adapted with permission from ref. 72. Copyright {2022} American Chemical Society. Reproduced from ref. 107 with permission from the Royal Society of Chemistry.

To avoid the adverse absorption of irradiation and emission of the metal shell existing in the metal shell-UCNPs core structure, some researchers fabricated metal particles as the core materials while UCNPs acted as the shell part. Fig. 12 displays a Ag core coated with SiO_2 isolation layers by Yin.[72] UCNPs were synthesized *in situ* from precursors ($LnCl_3$) in Ag@SiO_2 solution and precipitated on the surface to constitute the outermost shell. The absorption spectrum ensured the SPR effect of the Ag core, without a SiO_2@UCNPs peak being detected. Additionally, compared with pure Ag nanoparticles, Ag@SiO_2@UCNPs showed a redshift of the SPR wavelength from 350–665 nm to a broader range at 400–850 nm, resulting in a 30-fold enhancement of red emission under the excitation of 980 nm. Afterwards, Yin[107] carried out another attractive research work where Ag/graphene nanocomposites played the role of a core, while outside of a 10 nm thick SiO_2 isolation layer, the UCNP ($NaLuF_4$: Yb^{3+}, Gd^{3+}, Er^{3+}) shell existed. By graphene addition, the enhancement factor of the UCNPs-metal composites rose up to 52, and hence even higher than the former work.

Based on the core–shell mode, Hinamoto deposited a metal (Ag) cap above the Au-core@UCNPs-shell structures.[108] The Ag cap has a weak influence on the excitation enhancement of the SPR effect because of the mismatch of SPR peak at 735 nm and irradiation at 980 nm. Yet, the scattering wavelength of the Ag cap from 500 nm to 850 nm overlapped the emission bands of Au@UCNPs. Then the emission intensities of a number of Au@UCNPs and Ag-cap@UCNPs@Au nanoparticles were measured and shown in Fig. 13(b). Consequently, the average green
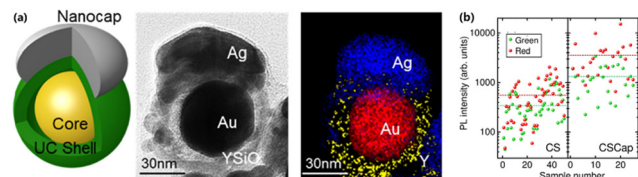

Fig. 13 (a) Schematic illustration, TEM image, EDS mapping image of Au core/Er^{3+} and Yb^{3+} co-doped yttrium silicate shell/Ag shell (CSCap) composite nanoparticles. (b) Upconversion PL peak intensities obtained for a 50 Au core/Er^{3+} and Yb^{3+} co-doped yttrium silicate shell (CS) and 24 CSCap particles. Adapted with permission from ref. 108. Copyright {2022} American Chemical Society.

This journal is © The Royal Society of Chemistry 2023

J. Mater. Chem. B, 2023, **11**, 5238–5250 | **5245**

and red emissions calculated were further enhanced by factors 3.5 and 6, respectively, by virtue of dual SPR–UCNP coupling.

However, chemical synthesis methods show disadvantages, like complex preparation processes. Besides, reaction parameters such as surfactant, reaction temperature, time or speed may exert effects on the surface defects of NPs.[109] So the enhancement factor is hard to catch up with that of the physical method.

Applications in bioimaging

On account of advances in the metal SPR effect enhancement on UCNPs photoluminescence intensity achieved in recent years, the application of plasmon resonance materials can be witnessed in solar cells,[110] photocatalysis,[111] anti-counterfeiting,[90] sensors,[112] photothermal therapy,[113] bioimaging[114] and other fields. Combined with our own research background, this review focuses on the application of SPR-enhanced upconversion luminescence in bioimaging.

The NaYF$_4$: Yb^{3+},Er^{3+}@SiO$_2$@Ag nanocomposites prepared by Yuan[104] exhibited an obvious upconversion luminescence enhancement because of the coupling between UCNPs and Ag nanoparticles, as mentioned in the Section "Chemical construction of SPR–UCNPs". The cytotoxicity of nanocomposites is weakened through the modification with DNA materials, seen from the increase of cell viability from 50% to 92% after 24 h incubation in Fig. 14. After co-incubation with murine melanoma cells B16F0, confocal images showed bright green fluorescence corresponding to the emission band of Er^{3+} ($^4S_{3/2}$–$^4I_{15/2}$) inside the cells under the excitation of 980 nm at 500 mW power. The irradiation led to little cellular lethality only, confirming the potential of NaYF$_4$: Yb^{3+},Er^{3+}@SiO$_2$@Ag as an optical imaging agent.

Another kind of cancer cell line (HeLa), which is artificially cultured with infinite multiplication capacity, was first derived from cervical cancer from an American woman Henrietta Lacks, also known as experimental proliferating epidermal cancer cells. The studies on the fluorescence imaging ability of metal-UCNPs nanomaterials with HeLa cells *in vitro* have been carried out
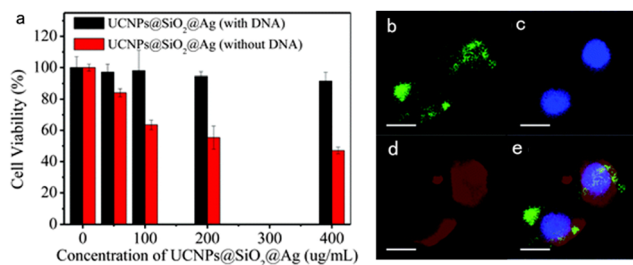

Fig. 14 (a) Viability of cells incubated with metal@UCNP nanocomposites before (red) and after (black) modification with DNA. (b) Upconversion luminescence image of live B16F0 cells after incubation with DNA-modified nanocomposites (green). (c and d) Fluorescence images of the cells counterstained with DAPI (blue) and Concanavalin A (red) to show the nucleus and cell membranes, respectively. The merged images are shown in (e). (Scale bar: 20 µm.) Reproduced from ref. 104 with permission from the Royal Society of Chemistry.
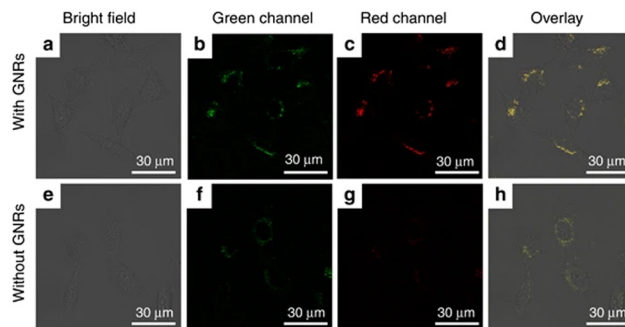

Fig. 15 Confocal laser scanning microscopy images of HeLa cells incubated with GNR@UCNPs hybrid nanostructures (top row: (a) bright field image; (b) green channel image; (c) red channel image and (d) overlay imaging.) and UCNPs (bottom row: (e) bright field image; (f) green channel image; (g) red channel image and (h) overlay imaging).[76]

abundantly over the past five years.[114–119] Observable upconversion fluorescence under near-infrared excitation is dependent on the lanthanide ions doped inside UCNPs. The inverted fluorescence microscope displayed prominent red and green signals inside HeLa cells under 980 nm laser,[120] corresponding to the energy level $^4F_{9/2}$–$^4I_{15/2}$ and $^4S_{3/2}$–$^4I_{15/2}$ of activator ions Er^{3+} doped in Au nanorods@NaGdF$_4$ hybrids with SPR enhancement,[114] separately. Furthermore, He[76] discovered that the enhancement factor of Au nanorods in red emission exceeds that in the green region. The overlay images of HeLa cells by confocal laser scanning microscopy displayed a color change from green when incubated with SiO$_2$@UCNPs to yellow after the incubation with modified Au nanorods, as shown in Fig. 15. Another important discovery in HeLa upconversion luminescence experiments was the uptake of metal-UCNP nanocomposites. Neither under the confocal microscope nor the inverted fluorescence microscope, researchers observed the fluorescence signals in the culture medium surrounding HeLa cells. However, the fluorescence distributed among cellular cytoplasm and nucleus randomly showed up.[115] Wang[114] demonstrated the continuous ingestion and accumulation of UNCPs coated with shell layer formed by Au nanorods, as incubation time with HeLa cells was prolonged. Furthermore, the quantitative calculation of the intracellular content of Au, determined by ICP-MS technique also ensured its accuracy. Cell uptake and a relatively long period of stay made metal-UCNP hybrid materials satisfy the basic requirements of *in vitro* and *in vivo* bioimaging.

Fig. 16 displays apparent green light located at the tumor site under near-infrared excitation (980 nm) which can downshift tissue overheating and autofluorescence interference. The green emission intensity reached the maximum of 4 h after the injection of Au nanorods @NaGdF$_4$: Yb^{3+},Er^{3+} in mice.[114] Considering the aspect ratio of Au nanorods, a low aspect ratio is beneficial to the transportation and uptake of nanomaterials. However, a high length-diameter ratio strengthens the longitudinal instead of the transverse SPR effect and enhances red emission. The red shift of the integral emission wavelength to the near-infrared region increases the penetration depth of upconversion imaging *in vivo* which was certified
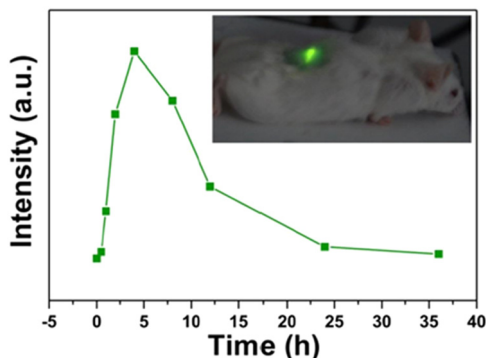
5246 | *J. Mater. Chem. B*, 2023, **11**, 5238–5250

This journal is © The Royal Society of Chemistry 2023

Fig. 16 The integrated intensity of UCL emission as a function of the tumor-bearing site injected time. (An *in vivo* merged images of a mouse injected with Au nanorods@UCNPs under NIR laser excitation is inset.)[114]

by Liu and co-workers.[113] After the modification with Au/Ag nanocages, $NaYF_4$: Yb^{3+}, Tm^{3+}@Yb^{3+}, Nd^{3+} nanoparticles exhibited yellow fluorescence penetration 2 mm deeper than unmodified ones in Fig. 17.

Apart from the fundamental upconversion luminescence property, metal-UCNP conjugates generally work as multifunctional contrast agents in the bioimaging field (Fig. 18).[121] Noble metals like Ag nanowires[119] turn out to be excellent computed tomographic (CT) agents with a Hounsfield unit (HU) value of 53.29 HU L g^{-1} which is almost twice as much as that of the commercial CT agent iohexol (29.67 HU L g^{-1})[122] because of high absorption of X-ray.[123] The Gd element doped in the metal-UCNPs composites has an intrinsic CT imaging performance but also shows a high magnetic resonance imaging (MRI) contrast either in T_1-weighted imaging[119] with relaxivity of 10.39 mM^{-1} s^{-1} or in T_2-weighted imaging[114] with 15.625 mM^{-1} s^{-1} relaxivity. It is unusual that the metal shell coating UCNP core structures attenuate imaging resolution mainly because the metals affect the paramagnetic properties of Gd-doped UCNPs. What is more, the addition of antibodies or targeting molecules towards metal-UCNPs composites prompts hybrids to act as bioimaging probes labelling tumor sites[9] or studying intermediate products of biological activities.[118]

Bioimaging is vital to the development of life sciences and medicine because of its ability to monitor various physiological and pathological processes in real-time with high clarity and visualize various biological entities. The metal SPR effect enhanced UCNPs photoluminescence with higher sensitivity
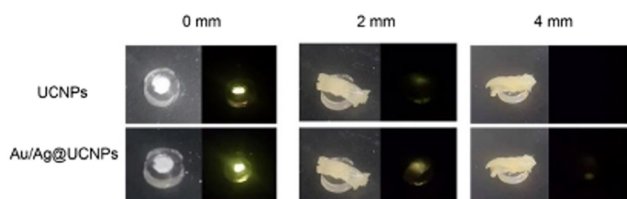

Fig. 18 *In vivo* multimodal imaging. (a) UCL imaging, (b) CT imaging, (c) photoacoustic imaging, and (d) T_1-MR imaging of HeLa tumor-bearing mice taken at different time points after injection with Au@UCNPs.[121]

is a promising strategy for applications in bioimaging. However, though Das[95] and Yin[92] respectively indicated that the SPR effect induced more intense enhancement to the photoluminescence of UCNPs at the lower excitation intensities compared with stronger irradiation, absolute emission intensities might be decreased because of less absorption. Therefore, it is significant to find the balance between the large enhancement factor by SPR effect and the high emission intensity of UCNPs at the safe dose[26] of 980 nm excitation (no more than 0.726 W cm^{-2}). Some researchers have realized this issue and mentioned it in the studies where the 980 nm laser intensity utilized is 600 mW cm^{-2} for the *in vitro* cellular experiments but is not indicated for *in vivo* bioimaging.[114,120] The question remains whether the bioimaging of UCNPs *in vivo* can be realized at a safe power density of 980 nm with the aid of the Au/Ag SPR effect, which is believed to be solvable.

Conclusion

UCNPs have low upconversion luminescence efficiency, limiting their further application. The UCNP luminescence can be effectively enhanced by the metal SPR effect. In this review, mechanisms of the SPR effect regulating UCNP luminescence, and preparation methods of the SPR–UCNP system along with its applications in the bioimaging field are elaborated in sequence.

Fig. 17 Penetration changes when UCNPs are modified with Au/Ag metals. Adapted with permission from ref. 113. Copyright {2022} American Chemical Society.
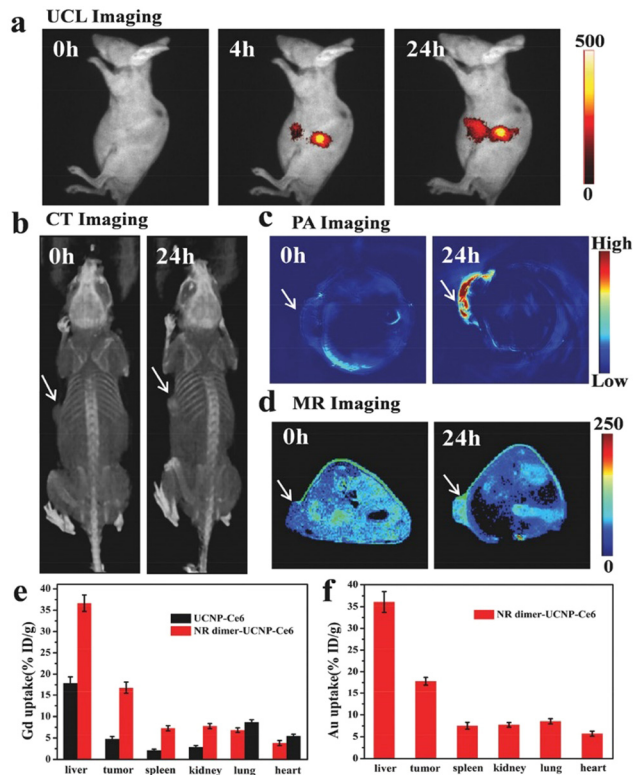
This journal is © The Royal Society of Chemistry 2023

J. Mater. Chem. B, 2023, **11**, 5238–5250 | **5247**

However, there are still some pressing issues in the field: (1) as photoluminescence enhancement involves the complex interaction of excitation light, rare earth ions and metal SPR in different states, there is still a lack of accepted theoretical models to explain the interaction mechanism between metal SPR and UCNPs. Therefore, the theory of UCNP luminescence enhanced by metal SPR needs to be further improved and corroborated in the experiment. (2) The chemical synthesis methods have complex steps, multiple reaction parameters along with limited enhancement factors while physical ones are mostly completed on a rigid substrate which results in poor biocompatibility. Therefore, how to prepare an effective and repeatable SPR–UCNP system is still a big challenge. (3) Compared with the preparation and mechanism research of the SPR–UCNP system, the application research in bioimaging of the SPR–UCNP system is relatively rare but has potential and is attractive.

Author contributions

Conflicts of interest

There are no conflicts to declare.

Acknowledgements

Notes and references

1 N. Bloembergen, *Phys. Rev. Lett.*, 1959, **2**, 84–85.
2 F. Auzel, *Chem. Rev.*, 2004, **104**, 139–173.
3 J. F.-C. Loo, Y.-H. Chien, F. Yin, S.-K. Kong, H.-P. Ho and K.-T. Yong, *Coord. Chem. Rev.*, 2019, **400**, 213042.
4 H. Dong, L.-D. Sun and C.-H. Yan, *Chem. Soc. Rev.*, 2015, **44**, 1608–1634.
5 B. Yang, H. Chen, Z. Zheng and G. Li, *J. Lumin.*, 2020, **223**, 117226.
6 H. S. Mader, P. Kele, S. M. Saleh and O. S. Wolfbeis, *Curr. Opin. Chem. Biol.*, 2010, **14**, 582–596.
7 Y. Fan, P. Wang, Y. Lu, R. Wang, L. Zhou, X. Zheng, X. Li, J. A. Piper and F. Zhang, *Nat. Nanotechnol.*, 2018, **13**, 941–946.
8 Y. Lu, J. Lu, J. Zhao, J. Cusido, F. M. Raymo, J. Yuan, S. Yang, R. C. Leif, Y. Huo, J. A. Piper, J. Paul Robinson, E. M. Goldys and D. Jin, *Nat. Commun.*, 2014, **5**, 3741.
9 G. Xiang, X. Liu, Q. Xia, X. Liu, S. Xu, S. Jiang, X. Zhou, L. Li, D. Wu, L. Ma, X. Wang and J. Zhang, *Talanta*, 2021, **224**, 121832.
10 N. Kang, Y. Liu, Y. Zhou, D. Wang, C. Chen, S. Ye, L. Nie and L. Ren, *Adv. Healthcare Mater.*, 2016, **5**, 1356–1363.
11 Y. Liu, N. Kang, J. Lv, Z. Zhou, Q. Zhao, L. Ma, Z. Chen, L. Ren and L. Nie, *Adv. Mater.*, 2016, **28**, 6411–6419.
12 Y. Luo, W. Zhang, Z. Liao, S. Yang, S. Yang, X. Li, F. Zuo and J. Luo, *Nanomaterials*, 2018, **8**, 466.
13 F. He, G. Yang, P. Yang, Y. Yu, R. Lv, C. Li, Y. Dai, S. Gai and J. Lin, *Adv. Funct. Mater.*, 2015, **25**, 3966–3976.
14 S. Chen, A. Z. Weitemier, X. Zeng, L. He, X. Wang, Y. Tao, A. J. Y. Huang, Y. Hashimotodani, M. Kano, H. Iwasaki, L. K. Parajuli, S. Okabe, D. B. L. Teh, A. H. All, I. Tsutsui-Kimura, K. F. Tanaka, X. Liu and T. J. McHugh, *Science*, 2018, **359**, 679–684.
15 Y. Ma, J. Bao, Y. Zhang, Z. Li, X. Zhou, C. Wan, L. Huang, Y. Zhao, G. Han and T. Xue, *Cell*, 2019, **177**, 243–255.
16 G. Chen, H. Qiu, P. N. Prasad and X. Chen, *Chem. Rev.*, 2014, **114**, 5161–5214.
17 Y. Ouyang, Y. Liu, Z. M. Wang, Z. Liu and M. Wu, *Nano-Micro Lett.*, 2021, **13**, 133.
18 M. Huang, L. Wang, X. Zhang, J. Zhou, L. Liu, Y. Pan, B. Yu and Z. Yu, *Nano*, 2017, **12**, 1750057.
19 D. T. Vu, T. T. Vu-Le, V. N. Nguyen, Q. M. Le, C.-R. C. Wang, L.-K. Chau, T.-S. Yang, M. W. Y. Chan, C.-I. Lee, C.-C. Ting, J.-Y. Lin, H.-C. Kan and C. C. Hsu, *Int. J. Smart Nano Mater.*, 2021, **12**, 49–71.
20 G. Yang, Y. Cao, B. Yan, Q. Lv, J. Yu, F. Zhao, Z. Chen, H. Yang, M. Chen and Z. Jin, *Oncotarget*, 2018, **9**, 16758–16774.
21 X. Zou, M. Xu, W. Yuan, Q. Wang, Y. Shi, W. Feng and F. Li, *Chem. Commun.*, 2016, **52**, 13389–13392.
22 D. M. Wu, A. García-Etxarri, A. Salleo and J. A. Dionne, *J. Phys. Chem. Lett.*, 2014, **5**, 4020–4031.
23 A. Gupta, S. Ghosh, M. K. Thakur, J. Zhou, K. Ostrikov, D. Jin and S. Chattopadhyay, *Prog. Mater. Sci.*, 2021, **121**, 100838.
24 G. Chen, T. Y. Ohulchanskyy, S. Liu, W.-C. Law, F. Wu, M. T. Swihart, H. Ågren and P. N. Prasad, *ACS Nano*, 2012, **6**, 2969–2977.
25 Z. Chen, W. Sun, H.-J. Butt and S. Wu, *Chem. – Eur. J.*, 2015, **21**, 9165–9170.
26 Laser Institute of America, *SPIE Medical Imaging*, 2007.
27 S. Wen, J. Zhou, K. Zheng, A. Bednarkiewicz, X. Liu and D. Jin, *Nat. Commun.*, 2018, **9**, 2415.
28 Q. Cheng, J. Sui and W. Cai, *Nanoscale*, 2012, **4**, 779–784.
29 Y. Sun, H. Bi, T. Wang, L. Sun, Z. Li, H. Song, F. Sun, H. Zhou, G. Zhou and J. Hu, *Mater. Sci. Eng., B*, 2020, **261**, 114674.

5248 | *J. Mater. Chem. B*, 2023, **11**, 5238–5250

This journal is © The Royal Society of Chemistry 2023

30 H. Lin, Z. Wang and Y. Hong, *J. Nanomater.*, 2020, **2020**, 8509380.

31 R. Luo, L. Chen, Q. Li, J. Zhou, L. Mei, Z. Ning, Y. Zhao, M. Liu, X. Lai, J. Bi, W. Yin and D. Gao, *Inorg. Chem.*, 2020, **59**, 17906–17915.

32 H. Rabie, Y. Zhang, N. Pasquale, M. J. Lagos, P. E. Batson and K.-B. Lee, *Adv. Mater.*, 2019, **31**, 1806991.

33 Z. Meng, S. Zhang and S. Wu, *J. Lumin.*, 2020, **227**, 117566.

34 B. Li, T. Gu, T. Ming, J. Wang, P. Wang, J. Wang and J. C. Yu, *ACS Nano*, 2014, **8**, 8152–8162.

35 Z. Yin, X. Zhang, D. Zhou, H. Wang, W. Xu, X. Chen, T. Zhang and H. Song, *RSC Adv.*, 2016, **6**, 86297–86300.

36 X. Chen, W. Xu, L. Zhang, X. Bai, S. Cui, D. Zhou, Z. Yin, H. Song and D.-H. Kim, *Adv. Funct. Mater.*, 2015, **25**, 5462–5471.

37 Q. Zhan, X. Zhang, Y. Zhao, J. Liu and S. He, *Laser Photonics Rev.*, 2015, **9**, 479–487.

38 B. Zhou, B. Shi, D. Jin and X. Liu, *Nat. Nanotechnol.*, 2015, **10**, 924–936.

39 D. Yang, C. Cao, W. Feng, C. Huang and F. Li, *J. Rare Earths*, 2018, **36**, 113–118.

40 W. Shao, G. Chen, A. Kuzmin, H. L. Kutscher, A. Pliss, T. Y. Ohulchanskyy and P. N. Prasad, *J. Am. Chem. Soc.*, 2016, **138**, 16192–16195.

41 H. Wang, Z. Wang, Y. Tu, Y. Li, T. Xu, M. Yang, P. Wang and Y. Gu, *Biomaterials*, 2020, **235**, 119765.

42 C. Liu, B. Liu, J. Zhao, Z. Di, D. Chen, Z. Gu, L. Li and Y. Zhao, *Angew. Chem., Int. Ed.*, 2020, **59**, 2634–2638.

43 G. Chen, T. Y. Ohulchanskyy, A. Kachynski, H. Ågren and P. N. Prasad, *ACS Nano*, 2011, **5**, 4981–4986.

44 C. Strohhofer and A. Polman, *J. Appl. Phys.*, 2001, **90**, 4314–4320.

45 D. Gao, X. Zhang and W. Gao, *ACS Appl. Mater. Interfaces*, 2013, **5**, 9732–9739.

46 H. Atwater and A. Polman, *Nat. Mater.*, 2010, **9**, 865.

47 H. Yang, L.-Q. He, Y.-W. Hu, X. Lu, G.-R. Li, B. Liu, B. Ren, Y. Tong and P.-P. Fang, *Angew. Chem., Int. Ed.*, 2015, **54**, 11462–11466.

48 S. K. Ghosh and T. Pal, *Chem. Rev.*, 2007, **107**, 4797–4862.

49 C. Cretu and E. van der Lingen, *Gold Bull.*, 1999, **32**, 115–126.

50 D. Compton, L. Cornish and E. van der Lingen, *Gold Bull.*, 2003, **36**, 10–16.

51 Y. A. Eremin, in *Encyclopedia of Modern Optics*, ed., R. D. Guenther, Elsevier, Oxford, 2005, pp. 326–330.

52 G. Mie, *Ann. Phys.*, 1908, **330**, 377–445.

53 D. Pines, *Rev. Mod. Phys.*, 1956, **28**, 184–198.

54 R. H. Ritchie, *Phys. Rev.*, 1957, **1**, 874–881.

55 C. Powell and J. Swan, *Phys. Rev.*, 1959, **116**, 81–83.

56 M. M. Alvarez, J. T. Khoury, T. G. Schaaff, M. N. Shafigullin, I. Vezmar and R. L. Whetten, *J. Phys. Chem. B*, 1997, **101**, 3706–3712.

57 P. Chang, K. Liu, J. Jiang, T. Xu, Z. Zhang, J. Ma, Y. Zhao, J. Zhang, X. Li and T. Liu, *Sens. Actuators, A*, 2020, **309**, 112022.

58 P. K. Baruah, A. K. Sharma and A. Khare, *Opt. Laser Technol.*, 2018, **108**, 574–582.

59 D. Mann, D. Nascimento-Duplat, H. Keul, M. Möller, M. Verheijen, M. Xu, H. P. Urbach, A. J. L. Adam and P. Buskens, *Plasmonics*, 2017, **12**, 929–945.

60 W. Feng, L.-D. Sun and C.-H. Yan, *Chem. Commun.*, 2009, 4393–4395.

61 W. Park, D. Lu and S. Ahn, *Chem. Soc. Rev.*, 2015, **44**, 2940–2962.

62 J. Shen, Z. Q. Li, Y. R. Chen, X. H. Chen, Y. W. Chen, Z. Sun and S. M. Huang, *Appl. Surf. Sci.*, 2013, **270**, 712–717.

63 K. Zheng, K. Y. Loh, Y. Wang, Q. Chen, J. Fan, T. Jung, S. H. Nam, Y. D. Suh and X. Liu, *Nano Today*, 2019, **29**, 100797.

64 G. Schneider, G. Decher, N. Nerambourg, R. Praho, M. H. V. Werts and M. Blanchard-Desce, *Nano Lett.*, 2006, **6**, 530–536.

65 S. Han, R. Deng, X. Xie and X. Liu, *Angew. Chem., Int. Ed.*, 2014, **53**, 11702–11715.

66 K. Aslan and C. D. Geddes, *Met.-Enhanced Fluoresc.*, 2010, pp. 1–23.

67 E. C. L. Ru, J. Grand, N. Félidj, J. Aubard, G. Lévi, A. Hohenau, J. R. Krenn, E. Blackie and P. G. Etchegoin, *Me.-Enhanced Fluoresc.*, 2010, pp. 25–65.

68 D. J. Ross, N. P. W. Pieczonka and R. F. Aroca, *Met.-Enhanced Fluoresc.*, 2010, pp. 67–90.

69 K. Munechika, Y. Chen, J. M. Smith and D. S. Ginger, *Met.-Enhanced Fluoresc.*, 2010, pp. 91–118.

70 W. Deng, F. Xie, H. T. M. C. M. Baltar and E. M. Goldys, *Phys. Chem. Chem. Phys.*, 2013, **15**, 15695–15708.

71 P. Xu, Q. Li, T. Li, W. Rao, Y. Wang, S. Lan and L. Wu, *Plasmonics*, 2014, **9**, 1039–1047.

72 D. Yin, C. Wang, J. Ouyang, X. Zhang, Z. Jiao, Y. Feng, K. Song, B. Liu, X. Cao, L. Zhang, Y. Han and M. Wu, *ACS Appl. Mater. Interfaces*, 2014, **6**, 18480–18488.

73 Q.-C. Sun, H. Mundoor, J. C. Ribot, V. Singh, I. I. Smalyukh and P. Nagpal, *Nano Lett.*, 2014, **14**, 101–106.

74 A. Priyam, N. M. Idris and Y. Zhang, *J. Mater. Chem.*, 2012, **22**, 960–965.

75 F. Kang, J. He, T. Sun, Z. Y. Bao, F. Wang and D. Y. Lei, *Adv. Funct. Mater.*, 2017, **27**, 1701842.

76 J. He, W. Zheng, F. Ligmajer, C.-F. Chan, Z. Bao, K.-L. Wong, X. Chen, J. Hao, J. Dai, S.-F. Yu and D. Y. Lei, *Light: Sci. Appl.*, 2017, **6**, e16217.

77 A. L. Feng, M. Lin, L. Tian, H. Y. Zhu, H. Guo, S. Singamaneni, Z. Duan, T. J. Lu and F. Xu, *RSC Adv.*, 2015, **5**, 76825–76835.

78 Y. Xue, C. Ding, Y. Rong, Q. Ma, C. Pan, E. Wu, B. Wu and H. Zeng, *Small*, 2017, **13**, 1701155.

79 D. Mendez-Gonzalez, S. Melle, O. G. Calderón, M. Laurenti, E. Cabrera-Granado, A. Egatz-Gómez, E. López-Cabarcos, J. Rubio-Retama and E. Díaz, *Nanoscale*, 2019, **11**, 13832–13844.

80 R. Lv, F. Yang, X. Jiang, B. Hu, X. Zhang, X. Chen and J. Tian, *J. Lumin.*, 2020, **220**, 116974.

81 Y. Qin, Z. Dong, D. Zhou, Y. Yang, X. Xu and J. Qiu, *Opt. Mater. Express*, 2016, **6**, 1942–1955.

82 H. Wang, J. Cui, Z. Zheng, Q. Shi, T. Sun, X. Liu, Q. Huang and T. Fukuda, *ACS Appl. Mater. Interfaces*, 2017, **9**, 41669–41679.

83 F. Xu, H. Gao, J. Liang, S. Jin, J. Zhao, Y. Liu, H. Zhang, Z. Zhang and Y. Mao, *Ceram. Int.*, 2019, **45**, 21557–21563.

84 L. Lin, Z. Yu, Z. Wang, Z. Feng, F. Huang, L. Huang, Q. Dai, F. Zhang and Z. Zheng, *J. Lumin.*, 2019, **214**, 116598.

85 C. Zhao, N. Chen, S. Liu, Z. Chen and T. Wang, *J. Phys. Conf. Ser.*, 2017, **844**, 012055.

86 W. Zhang, J. Li, H. Lei and B. Li, *ACS Appl. Mater. Interfaces*, 2017, **9**, 42935–42942.

87 B. Shao, Z. Yang, J. Li, J. Yang, Y. Wang, J. Qiu and Z. Song, *Opt. Mater. Express*, 2017, **7**, 1188–1197.

88 L. Wang and Y. Li, *Chem. Mater.*, 2007, **19**, 727–734.

89 G. Y. Lee, K. Jung, H. S. Jang, J. Kyhm, I. K. Han, B. Park, H. Ju, S. J. Kwon and H. Ko, *Nanoscale*, 2016, **8**, 2071–2080.

90 H. Liu, J. Xu, H. Wang, Y. Liu, Q. Ruan, Y. Wu, X. Liu and J. K. W. Yang, *Adv. Mater.*, 2019, **31**, 1807900.

91 J. Dong, W. Gao, Q. Han, Y. Wang, J. Qi, X. Yan and M. Sun, *Rev. Phys.*, 2019, **4**, 100026.

92 Z. Yin, D. Zhou, W. Xu, S. Cui, X. Chen, H. Wang, S. Xu and H. Song, *ACS Appl. Mater. Interfaces*, 2016, **8**, 11667–11674.

93 M. Saboktakin, X. Ye, U. K. Chettiar, N. Engheta, C. B. Murray and C. R. Kagan, *ACS Nano*, 2013, **7**, 7186–7192.

94 S. Zhan, J. Xiong, G. Nie, S. Wu, J. Hu, X. Wu, S. Hu, J. Zhang, Y. Gao and Y. Liu, *Adv. Mater. Interfaces*, 2019, **6**, 1802089.

95 A. Das, C. Mao, S. Cho, K. Kim and W. Park, *Nat. Commun.*, 2018, **9**, 4828.

96 A. Chu, H. He, Z. Yin, R. Peng, H. Yang, X. Gao, D. Luo, R. Chen, G. Xing and Y. J. Liu, *ACS Appl. Mater. Interfaces*, 2020, **12**, 1292–1298.

97 W. Gao, B. Y. Wang, Q. Y. Han, S. S. Han, X. T. Cheng, C. X. Zhang, Z. Y. Sun, L. Liu, X. W. Yan, Y. K. Wang and J. Dong, *Acta Phys. Sin.*, 2020, **69**, 184213.

98 E. Verhagen, L. Kuipers and A. Polman, *Opt. Express*, 2009, **17**, 14586–14598.

99 S. K. Maurya, S. P. Tiwari, A. Kumar and K. Kumar, *J. Rare Earths*, 2018, **36**, 903–910.

100 X. Chen, D. Peng, Q. Ju and F. Wang, *Chem. Soc. Rev.*, 2015, **44**, 1318–1330.

101 G.-S. Yi and G.-M. Chow, *Chem. Mater.*, 2007, **19**, 341–343.

102 H. Zhang, Y. Li, I. A. Ivanov, Y. Qu, Y. Huang and X. Duan, *Angew. Chem., Int. Ed.*, 2010, **49**, 2865–2868.

103 Y. Ding, X. Zhang, H. Gao, S. Xu, C. Wei and Y. Zhao, *J. Lumin.*, 2014, **147**, 72–76.

104 P. Yuan, Y. H. Lee, M. K. Gnanasammandhan, Z. Guan, Y. Zhang and Q.-H. Xu, *Nanoscale*, 2012, **4**, 5132–5137.

105 W. Xu, X. Chen and H. Song, *Nano Today*, 2017, **17**, 54–78.

106 W. Deng, L. Sudheendra, J. Zhao, J. Fu, D. Jin, I. M. Kennedy and E. M. Goldys, *Nanotechnology*, 2011, **22**, 325604.

107 D. Yin, X. Cao, L. Zhang, J. Tang, W. Huang, Y. Han and M. Wu, *Dalton Trans.*, 2015, **44**, 11147–11154.

108 T. Hinamoto, H. Sugimoto and M. Fujii, *J. Phys. Chem. C*, 2018, **122**, 17465–17472.

109 W. Xu, S. Xu, Y. Zhu, T. Liu, X. Bai, B. Dong, L. Xu and H. Song, *Nanoscale*, 2012, **4**, 6971–6973.

110 Y. Ding, H. Qiao, T. Yang, N. Yin, P. Li, Y. Zhao and X. Zhang, *Opt. Mater.*, 2017, **73**, 617–622.

111 Z. Zhang, Y. Liu, Y. Fang, B. Cao, J. Huang, K. Liu and B. Dong, *Adv. Sci.*, 2018, **5**, 1800748.

112 K. Zhang, F. Lu, Z. Cai, S. Song, L. Jiang, Q. Min, X. Wu and J.-J. Zhu, *Anal. Chem.*, 2020, **92**, 11795–11801.

113 J. Liu, F. Yang, M. Feng, Y. Wang, X. Peng and R. Lv, *ACS Biomater. Sci. Eng.*, 2019, **5**, 5051–5059.

114 C. Wang, C. Xu, L. Xu, C. Sun, D. Yang, J. Xu, F. He, S. Gai and P. Yang, *J. Mater. Chem. B*, 2018, **6**, 2597–2607.

115 B. Kumar, A. Murali, I. Mattan and S. Giri, *J. Phys. Chem. B*, 2019, **123**, 3738–3755.

116 M. Kataria, K. Yadav, A. Nain, H.-I. Lin, H.-W. Hu, C. R. Paul Inbaraj, T.-J. Chang, Y.-M. Liao, H.-Y. Cheng, K.-H. Lin, H.-T. Chang, F.-G. Tseng, W.-H. Wang and Y.-F. Chen, *ACS Appl. Mater. Interfaces*, 2020, **12**, 19840–19854.

117 S. S. Syamchand, R. S. Aparna and G. Sony, *Microchim. Acta*, 2017, **184**, 2255–2264.

118 S. Ghosh, Y.-F. Chang, D.-M. Yang and S. Chattopadhyay, *Biosens. Bioelectron.*, 2020, **155**, 112115.

119 S. Yamini, M. Gunaseelan, G. A. Kumar, S. Singh, G. C. Dannangoda, K. S. Martirosyan, D. K. Sardar, S. Sivakumar, A. Girigoswami and J. Senthilselvan, *Microchim. Acta*, 2020, **187**, 317.

120 R. Lv, P. Yang, Y. Dai, S. Gai, F. He and J. Lin, *ACS Appl. Mater. Interfaces*, 2014, **6**, 15550–15563.

121 M. Sun, L. Xu, W. Ma, X. Wu, H. Kuang, L. Wang and C. Xu, *Adv. Mater.*, 2016, **28**, 898–904.

122 Z. Zhou, J. Xie, S. Ma, X. Luo, J. Liu, S. Wang, Y. Chen, J. Yan and F. Luo, *ACS Omega*, 2021, **6**, 10723–10734.

123 X. Hu, Y. Zhang, T. Ding, J. Liu and H. Zhao, *Front. Bioeng. Biotechnol.*, 2020, **8**, 990.

5250 | *J. Mater. Chem. B*, 2023, **11**, 5238–5250

This journal is © The Royal Society of Chemistry 2023